Strained silicon technology: Non-destructive nanoscale characterization through Tip-enhanced Raman Spectroscopy

Giancarlo La Penna, Chiara Mancini, Anacleto Proietti, Luca Buccini, Daniele Passeri, Narciso Gambacorti, Jérôme Richy, Marco Rossi

Special Issue

Applied Spectroscopy

www.s-a-s.org

Strained Silicon Technology: Non-Destructive High-Lateral-Resolution Characterization Through Tip-Enhanced Raman Spectroscopy

Applied Spectroscopy
1–11

DOI: 10.1177/00037028241246292
journals.sagepub.com/home/asp
Sage

Giancarlo La Penna[1], Chiara Mancini[1], Anacleto Proietti[1], Luca Buccini[1], Daniele Passeri[1,2], Narciso Gambacorti[3], Jérôme Richy[3], and Marco Rossi[1,2]

Abstract

The semiconductor industry is undergoing a transformative phase, marked by the relentless drive for miniaturization and a constant demand for higher performance and energy efficiency. However, the reduction of metal–oxide–semiconductor field-effect transistor sizes for advanced technology nodes below 10 nm presents several challenges. In response, strained silicon technology has emerged as a key player, exploiting strain induction in the silicon crystal lattice to improve device performance. At the same time, there has been a growing need for characterization techniques that allow in-line monitoring of sample conditions during semiconductor manufacturing, as an alternative to traditional methods such as transmission electron microscopy or high-resolution X-ray diffraction, which have several limitations in terms of measurement time and sample destructiveness. This paper explores the application of advanced spectroscopic characterization techniques, in particular μ-Raman spectroscopy and tip-enhanced Raman spectroscopy (TERS), to meet the evolving needs of the semiconductor industry for quality control and failure analysis, increasingly requiring faster and non-destructive characterization techniques. μ-Raman provides insight into strain values and distributions of strained layers with different thicknesses and germanium concentrations, but its lateral resolution is constrained by the Abbe diffraction limit. TERS, on the other hand, emerges as a powerful non-destructive technique capable of overcoming diffraction limits by exploiting the combination of an atomic force microscope with a Raman spectrometer. This breakthrough makes it possible to estimate the chemical composition and induced strain in the lattice by evaluating the Raman peak position shifts in strained and unstrained silicon layers, providing crucial insights for nanoscale strain control. In particular, this paper focuses on the TERS characterization of $Si_{0.7}Ge_{0.3}$ epitaxial layers grown on a silicon-on-insulator device, demonstrating the effectiveness of this technique and the high lateral resolution that can be achieved.

Keywords

Micro-Raman Spectroscopy, tip-enhanced Raman Spectroscopy, TERS, strain and stress, strained silicon, silicon–germanium, SiGe, epitaxial-on-silicon-on-insulator, SOI, semiconductors, nanoelectronic devices, nanoscale

Date received: 24 December 2023; accepted: 21 March 2024

Introduction

The continuing trend of shrinking and miniaturization of semiconductor devices is driving information processing technology into a wider range of new applications and capabilities. Therefore, the current demands of the semiconductor industry to reduce the size of metal–oxide–semiconductor field-effect transistor (MOSFET) transistors below 10 nm[1,2] leads to various consequences, ranging from quantum mechanical and thermal effects to the growing complexity of the device fabrication. To overcome these challenges, strained silicon technology is having a great impact in the field of integrated circuits, offering major advantages, particularly in terms of miniaturization.[3,4] This technology is

[1]Department of Basic and Applied Sciences for Engineering, Sapienza University of Rome, Rome, Italy
[2]Research Center for Nanotechnology Applied to Engineering of Sapienza (CNIS), Sapienza University of Rome, Rome, Italy
[3]Univ Grenoble Alpes, CEA, Leti, Grenoble, France

Corresponding Author:
Marco Rossi, Department of Basic and Applied Sciences for Engineering, Sapienza University of Rome, Via A. Scarpa 16, 00161 Rome, Italy.
Email: marco.rossi@uniroma1.it

based on introducing stress into the silicon crystal lattice in specific regions of a MOSFET, to improve the performance and energy efficiency of the device, such as significantly enhanced carrier mobility, increased on-current, and reduced off-state leakage current.[5] One of the most common strained silicon structures in the semiconductor industry is represented by $Si_{1-x}Ge_x$ thin epitaxial layers grown on silicon-on-insulator (SOI) by chemical vapor deposition (CVD) or molecular beam epitaxy techniques.[6,7] This technology introduces compressive or tensile mechanical stress in the grown layer and in the bulk silicon underneath thanks to the lattice mismatch between silicon and germanium, which has a larger lattice constant. During the process, $Si_{1-x}Ge_x$ directly on SOI is obtained by a controlled amount (x) Ge-enrichment, introducing different levels of strain into the structure. The stress imposed must not be excessive to avoid self-relaxation defects in the silicon crystal, which would lead to dislocations and degradation of the device.

Therefore, there is an increasing need for fine strain control to predict the final properties of the device. The critical downscaling of nanoelectronic devices and the production of new nanostructured materials require the use of advanced high-resolution characterization techniques, as well as the development of innovative measurement approaches and robust nanometrological protocols. Among the various techniques available, those based on transmission electron microscopy[8–10] and high-resolution X-ray diffraction[11–13] have been the reference standard for the analysis of nano-deformations thanks to their high resolution, high sensitivity, and precision, but they also present several drawbacks, e.g., they are destructive, expensive, require long and precise protocols for sample preparation, and also they can fail in the highly stressed active regions of devices. For the reasons explained, especially in the case of nanoelectronics devices, there has been a growing need to employ faster and non-destructive characterization techniques in order to guarantee an in-line monitoring of strained silicon structures during the production processes while avoiding any kind of additional artifacts. This paper aims to show how optical spectroscopic techniques such as μ-Raman and tip-enhanced Raman spectroscopy (TERS) have excellent potential to be considered reliable and precise non-destructive tools for strain characterization of strained silicon-based devices.[14] The case study of this work is a thin $Si_{0.7}Ge_{0.3}$ layer (17 nm) epitaxially grown on SOI. It has been produced to investigate the effect of the process parameters and has a certain industrial relevance as a standard sample in the semiconductor industry for exploring new device architectures and technologies. In fact, the SiGe on SOI substrate structure is known for its ability to enhance the performances of silicon-based devices since it shows superior carrier mobility compared to pure silicon, enables faster switching speeds, improves transistor performances, reduces parasitic capacitance, and lowers the power consumption, while improving radiation hardness. Therefore, this sample shows the ideal features to evaluate TERS as a potential tool to be integrated as an in-line technique for real-time monitoring of advanced semiconductor devices.

Indeed, the Raman Si–Ge vibrational modes are sensitive to strain as a function of the penetration depth of the excitation laser employed. However, the main drawback of the conventional μ-Raman spectroscopy is represented by its lateral resolution that is constrained by the Abbe diffraction limit,[15] in which the diameter of the laser beam spot limits the characterization to several hundreds of nanometers. For this reason, TERS is employed to carry out strain detection. Conceptually introduced for the first time in 1985 (demonstrating how surface-confined optical fields permit a new optical microscopy),[16] but only experimentally developed in 2000,[17–20] TERS is currently one of the most powerful methods for chemical analysis at the nanoscale in many different fields of application.[21,22] In this regard, in addition to the importance of TERS as a valuable instrument for the characterization of traditional semiconductor materials such as those discussed in this paper (Si–SiGe-based devices), in recent years, it has also proven to be an effective tool in the context of the nanoscale characterization of novel semiconductor materials such as single layer transition metal dichalcogenides and organic solar cells.[23–25] This technique combines the high spatial resolution of an atomic force microscope (AFM) with the high chemical sensitivity of a Raman spectrometer.[26,27] The AFM–TERS tip, usually noble metal-coated, acts as an antenna, both as a receiver of the Raman spectrometer light source and as a transmitter of the Raman signal from the region of the sample immediately beneath the probe. In the small gap between the tip and the sample (defined as a hotspot), not only a significant increase in signal intensity can be achieved, but also a great enhancement of the emission of the very surface of the sample, which is otherwise masked by the signal of the deep, bulk material underneath. The following analysis is composed of a preparatory characterization of the $Si_{0.7}Ge_{0.3}$ epitaxial-on-SOI sample in μ-Raman configuration, performed with two different wavelengths (532 and 355 nm) to unveil the physical limits of the technique; then the analyses in TERS mode are presented, where the 532 nm laser is combined with a titanium nitride (TiN)-coated TERS tip. It represents an innovative, refractory, and promising alternative probe that shows the plasmonic resonance frequency in the visible range of light and is compatible with standard silicon manufacturing facilities, i.e., clean room environments.[28–32] In TERS, the shifts of the Raman peak positions in the spectra of the strained (SiGe) and unstrained (Si substrate) regions of the sample are evaluated and analyzed in detail, demonstrating how this technique can become extremely important, especially in terms of lateral resolution and surface sensitivity.

Materials and Methods

Description of SiGe Epitaxial-on-SOI Device

The device analyzed, shown in Figure 1a, consists of a SOI substrate with a 12 nm Si film and a 25 nm thin SiO_2 BOX,

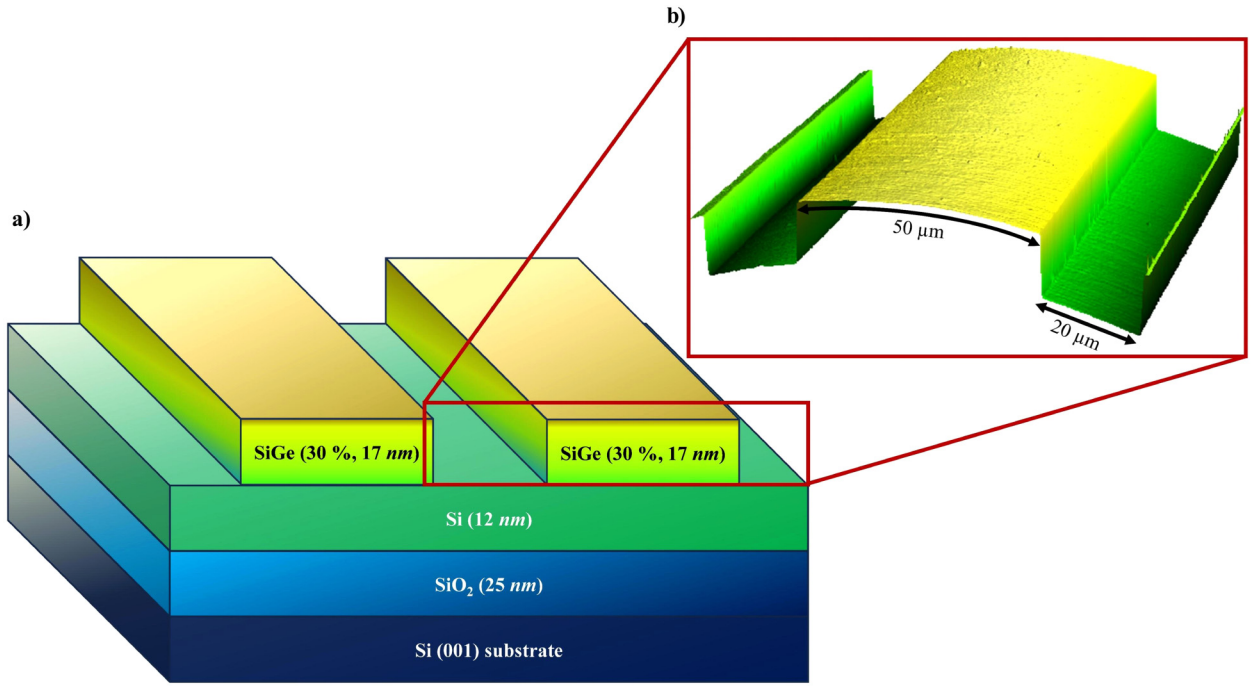

Figure 1. (a) Schematic reproduction of the analyzed section of the $Si_{0.7}Ge_{0.3}$ epitaxial-on-SOI device; (b) three-dimensional view of the topography of the section, with a detailed description of its features (SiGe and Si regions are 50 and 20 μm wide, respectively).

on which a 17 nm thin $Si_{1-x}Ge_x$ layer is grown by epitaxy according to several patterns with a targeted Ge concentration (x) of 30% by CVD. The device features a (001) bulk silicon substrate and the pattern consists of matrices of lines, squares, or rectangles periodically repeated with different dimensions and spacings (from 80 nm to 25 μm). For this study, the analyses are focused on a precise section of the sample, defined by parallel Si and SiGe lines with a width of 20 and 50 μm, respectively, as shown in Figure 1b.

Micro-Raman (μ-Raman) Spectroscopy

The sample was characterized using a confocal InVia Raman Spectrometer (Renishaw), with a 250 mm focal length. The analyses have been conducted at room temperature in the 100–700 cm^{-1} spectral range. The signal was dispersed by a holographic grating of 1800 L/mm and collected by a Peltier-cooled charge-coupled device detector. Two continuous-wave diode-pumped solid-state lasers are used to excite the sample: the first one at $\lambda = 532.1$ nm using a neodymium-doped yttrium aluminum garnet (Nd:YAG) laser (Renishaw) with a nominal power of 50 mW and focused on the sample through a short distance working objective N Plan 50×, with numerical aperture (NA) = 0.75 (Leica Microsystems); the second one at $\lambda = 354.8$ nm (Zouk from the Cobolt 05-01 series) with a power of 7 mW, focused on the sample using a 40× short working distance objective with NA = 0.47 (ThorLabs). The spectra have been normalized at 1 for a clearer interpretation of results and comparisons. The normalization procedure has been conducted on each spectrum with the software WiRE (v.4.4, from Renishaw) performing the ratio between each acquisition point and the value of its most intense peak.

Atomic Force Microscopy (AFM)

The topographies were acquired using a Dimension Icon AFM (Bruker) in tapping mode with RTESPA-300 (Bruker) tips with a spring constant of 40 N/m and a nominal first resonance frequency of 300 kHz. Gwyddion software (v.2.6, www.gwyddion.net) was used to analyze the images and reconstruct the three-dimensional structure. To reduce artifacts, the images were minimally processed by removing line coupling, compensating for substrate tilt, and removing an average plane.

Tip-Enhanced Raman Spectroscopy (TERS)

The TERS characterization was performed employing the same spectrometer of the μ-Raman characterization and 532 nm beam but using a 50× M Plan Apo SL type long working distance magnification objective (NA = 0.42, Leica Microsystems). The spectrometer is combined with a Bruker Innova AFM.[33] The TERS tips employed are innovative material TiN-coated silicon cantilevers (ScanSens GmbH), which are used in tapping mode. The Lorentzian fitting performed on TERS spectra has been performed with the software Origin Pro (2022 version).

Results and Discussion

Micro-Raman Spectroscopy Characterization

The first step of the work is the μ-Raman characterization of the SiGe epitaxial-on-SOI device in order to easily evaluate the standard technique capability, and so to demonstrate why an advanced tool such as TERS is strictly needed. In a typical Stokes Raman spectrum of the strained $Si_{1-x}Ge_x$ alloy, three well-defined peaks appear at ≈520, ≈411, and ≈300 cm^{-1} corresponding to the so-called Si–Si, Si–Ge, and Ge–Ge vibrational stretching modes, respectively.[34–36] Their presence, as well as their spectral position and intensity, depend strongly on both the thickness of the layer and its germanium content, thus on the induced strain. Different models allow one to predict the shift those peaks undergo because of the induced strain, depending on whether the SiGe structure is fully relaxed or fully strained.[37–42] The most relevant Raman peak in this case study is the one at ≈520 cm^{-1}, which represents the main vibrational mode of silicon in relaxed conditions. Its spectral position enables the easy detection of strain, since it is a vibrational mode sensitive to the presence (or absence) of stress: in the case of compression, the main silicon band appears at higher wavenumbers, while it is shifted to lower values when tensile stress is applied to the silicon lattice. The focus of this characterization is on the spectral region below 520 cm^{-1}, being the sample in a tensile state due to the germanium concentration equal to 30% in the SiGe layer. For this type of analysis, not only the resolution of the instrument is critical, but also the choice of the excitation wavelength, i.e., how deep the signal is collected in the sample, and its incident power. Two different excitation lasers were used to carry out Raman acquisitions, one in the visible (532 nm) and one in the near-ultraviolet (NUV; 355 nm) range, because of their very different penetration depth in this specific sample (≈200 nm in the case of the green laser, few nanometers in the NUV).[43] In both cases, the signal was acquired with localized, point measurements on the two distinct regions of the sample (Figure 2a). The point measurements have been intentionally acquired in the center of the

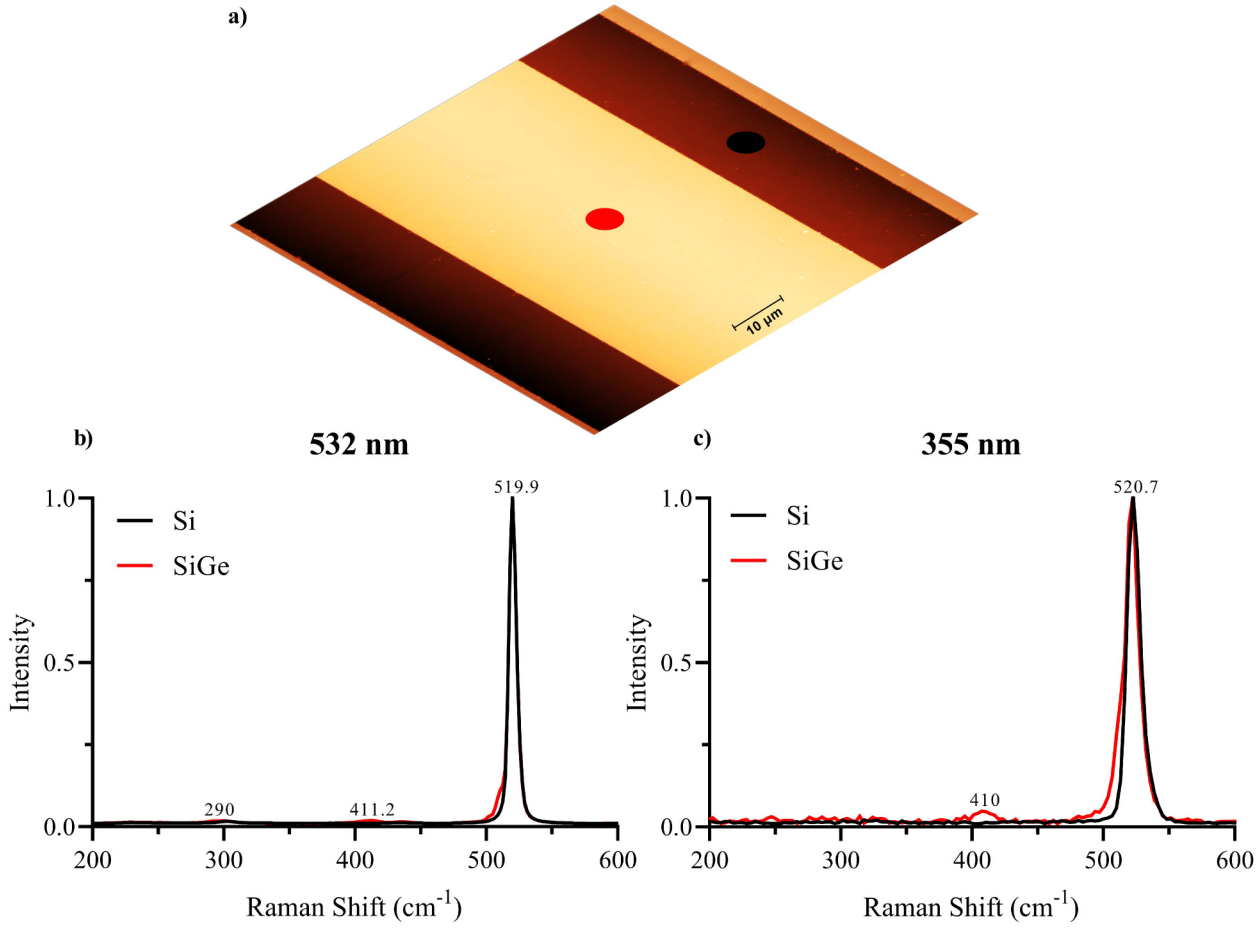

Figure 2. (a) Schematic of the section and the position of the point measurements on the two different regions, i.e., SiGe (red spot) and Si (black spot); (b, c) comparison between local Raman acquisitions collected from the two different regions (SiGe in red and Si in black) with the 532 nm and 355 nm excitation wavelengths, respectively.

two respective regions of the sample in order to avoid signal contamination in the spectrum from neighboring areas. The results obtained by employing the 532 nm laser are reported in Figure 2b, as a comparison between two normalized spectra. It can be easily seen that the acquisitions from the SiGe (red spectrum) and Si (black spectrum) sections report one distinct signal of the main vibrational mode of silicon, and they almost overlap. Anyway, as expected, in the SiGe spectrum, there is indeed a broadened peak below 520 cm^{-1}, indicating the presence of strain in the silicon lattice.[44,45] The NUV excitation laser (355 nm) is then used, which is considered more suitable for characterizing such a thin film because of its penetration depth.[46] In this case, the contribution of the strained layer is even more pronounced (Figure 2c): the spectrum acquired from the SiGe region is characterized by a very broad peak at ≈520 cm^{-1}, suggesting clearly the presence of a stress inside the lattice of the sample.

The results show that the interaction of this type of sample with the green and NUV excitation lasers produces spectra containing all the characteristic peaks of a typical Stokes Raman spectrum of $Si_{1-x}Ge_x$ alloys with these features (30% germanium content, 17 nm thickness). In particular, even if the strained-silicon signal appears very weak, the broadening of the main peak around 520 cm^{-1} indeed suggests the presence of a deformation in the crystal structure, more visible in the NUV case. In order to apply one of the models available to correlate the Raman shift of the strained-Si peak and strain percentage in the lattice, the accurate spectral positions of both the unstrained and strained silicon signals are required. A fitting procedure on the spectra acquired with the two excitation wavelengths is performed through Lorentzian curves in order to extract such data from the spectra and uncover how both the main peak broadening and position are affected by the stress imposed (Figure S1 and S2, respectively, Supplemental Material).

What emerges from the fitting procedure is that two Lorentzian curves are needed to fit the main silicon peak in the spectra acquired from the unstrained-Si region, regardless of the excitation laser employed: both peaks are related to the vibrational modes of relaxed-Si and appear at ≈521.7 and ≈519 cm^{-1} if the green laser is used, ≈525 and ≈521 cm^{-1} in the NUV case. In the strained-Si region, an additional Lorentzian curve has to be included in the fitting procedure, being it is related to the strained lattice and with a frequency position clearly shifted with respect to that of the main Si peak: it appears at ≈509.1 or ≈511.8 cm^{-1} if the laser used is the green or NUV one, respectively.

Pure silicon normally shows a dominant, sharp, and distinctive band at ≈520.7 cm^{-1} corresponding to the first-order optical phonon vibrational mode; in this case, the main peak appears broader and asymmetric in its right shoulder even in the unstrained Si region, most probably because of the several surface manufacturing processes that silicon undergoes during sample production, inducing defectivities in its crystal structure.[47] This effect emerges as a distinct second peak under the main silicon band, more precisely at ≈521.7 cm^{-1} for the green laser and even more visible at ≈525 cm^{-1} for the NUV one, due to its sensitivity to the surface of the sample. This interpretation explains the need to employ two curves for peak fitting to capture the observed spectral features accurately, in order to complete a purely mathematical procedure.

These acquisitions show a limitation of conventional μ-Raman spectroscopy, particularly concerning the penetration depth of the laser employed. The depth of the acquired signal is primarily constrained by factors such as the wavelength of the laser and its interaction with the sample, which dictate the penetration depth of the incident photons. Consequently, the Raman signal obtained reflects the scattering properties of a specific region within the sample. In this case, higher wavelengths (i.e., green laser) result in greater penetration depth, thereby reducing the surface sensitivity of the acquisition process in the very thin SiGe epitaxial layer-on-SOI structure; on the other hand, at lower wavelengths, i.e., NUV laser, the depth of the analysis is too low to collect enough signal from both the unstrained- and strained-Si regions for a reliable spectra comparison.

Thus, the laser employed clearly determines the Raman scattering efficiency and consequently the detection limit in samples based on SiGe alloys.[48] A careful TERS analysis could improve this characterization procedure and lead to a better understanding of the intricate relationship between germanium concentration and induced strain in the very thin SiGe layer thanks to its surface sensitivity to crystallinity deformations and lattice mismatches due to the device processing. Lastly, it is also important to remember that another main limitation of the conventional μ-Raman spectrometer is the lateral resolution of the technique. Due to the wave nature of light, diffraction defines the size of the laser spot focused on the sample, thus imposing a lateral resolution of several hundred nanometers,[15] considering that the maximum theoretical limit is approximately half the value of the excitation wavelength. For these reasons, the advanced TERS technique is employed to overcome all the drawbacks of standard μ-Raman spectroscopy.

Tip-Enhanced Raman Spectroscopy (TERS) Characterization

The second part of this work is focused on the TERS characterization of the device using a $\lambda = 532$ nm excitation wavelength at 5% of laser power. These parameters proved to be a suitable combination for the TiN-coated TERS tips, an innovative, refractory, and promising plasmonic material.[28–32] The wavelength where the maximum plasmonic resonance of titanium nitride is achieved is actually slightly higher than the excitation line used. However, although the plasmonic effect of TiN tips can be considered lower than that of conventional noble metal-coated ones when excited by the green laser,[30]

the properties of the probe employed, combined with its sharp geometry (which also enables a strong lightening rod effect), allow excellent performances in terms of field enhancement and Raman signal yield. The common procedure in TERS experiments is based on the acquisition of spectra on the area of interest of the sample in two configurations, "tip-in" and "tip-out". The first one allows us to collect the so-called near-field signal, which is emitted by the sample when illuminated by the electromagnetic field enhanced by the tip–laser interaction, being the probe engaged to the sample. This signal is not only very intense, but it is also emitted mostly from the surface of the sample, which is the region where plasmonic resonance between tip and laser takes place. On the other hand, the second configuration can be considered a conventional μ-Raman acquisition (far field), since the tip is removed from the line of sight of the laser and withdrawn from the sample surface. Still, the beam maintains the alignment on the sample of the tip-in acquisition. In this way, two spectra are acquired on the same point of the sample, containing two different information, i.e., one sensitive to its surface (near-field) and one related to the bulk composition (far-field).

The sample was subjected to TERS acquisition of different maps, profiles, and local measurements in the different areas to ensure repeatability and consistency of results. Figure 3a shows the comparison between the tip-in and tip-out TERS spectra acquired on the SiGe region. Here the spectra are intentionally not normalized in order to fully appreciate the enhancement in terms of signal intensity. In order to highlight the surface sensitivity of TERS, a comparison between spectra obtained from Si and SiGe regions in tip-in configuration is shown in Figure 3b. The spectrum acquired on the strained region shows the expected broadening below the main silicon band at ≈520 cm^{-1}, demonstrating that TERS could be able to detect the presence of stress. On the contrary, the spectrum from the relaxed region is perfectly symmetrical, as expected for pure silicon.

To accurately assess the performance of TERS tips for this kind of characterization, two important factors can be used to evaluate the effectiveness of electric field enhancement, i.e., contrast (C) and enhancement factor (EF).[21,49–51] The contrast is described by the following Eq. 1:

$$\text{Contrast (C)} = \frac{I_{\text{near field}}}{I_{\text{far field}}} = \frac{I_{\text{total}}}{I_{\text{far field}}} - 1 \quad (1)$$

where $I_{\text{near field}}$ is defined as the Raman peak intensity due only to the interaction of the tip with the scattering material and $I_{\text{far field}}$ is the intensity measured without the tip enhancement. The same formula can be expressed in terms of I_{total}, i.e., the signal while the tip is interacting with the sample ($I_{\text{tip-in}}$), which describes the value of the sum of the near- and far-field signal intensities.

Using the values obtained for I_{total} and $I_{\text{far field}}$ into Eq. 1, the resulting contrast is shown in Eq. 2:

$$\text{Contrast}_{(\text{SiGe})}(\text{C}) = \frac{I_{\text{total}}}{I_{\text{far field}}} - 1 = \frac{23\,834}{527} - 1 \approx 44.23 \quad (2)$$

Taking into consideration the contrast value, it is possible to calculate the EF through the following Eq. 3:

$$\text{EF} = C\left(\frac{V_{\text{far}}}{V_{\text{near}}}\right) \quad (3)$$

The EF is therefore calculated as the product between the contrast and the ratio between the scattering volume contributing to the far field (V_{far}, related to the radius of the laser spot focused on the sample) and near field (V_{near}, related to the radius of the apex of the tip used) signal intensities. In real working cases, as considered by Kumar et al.,[49] for a sufficiently thin film, these volumes included in the EF formula can be approximated to their corresponding areas,

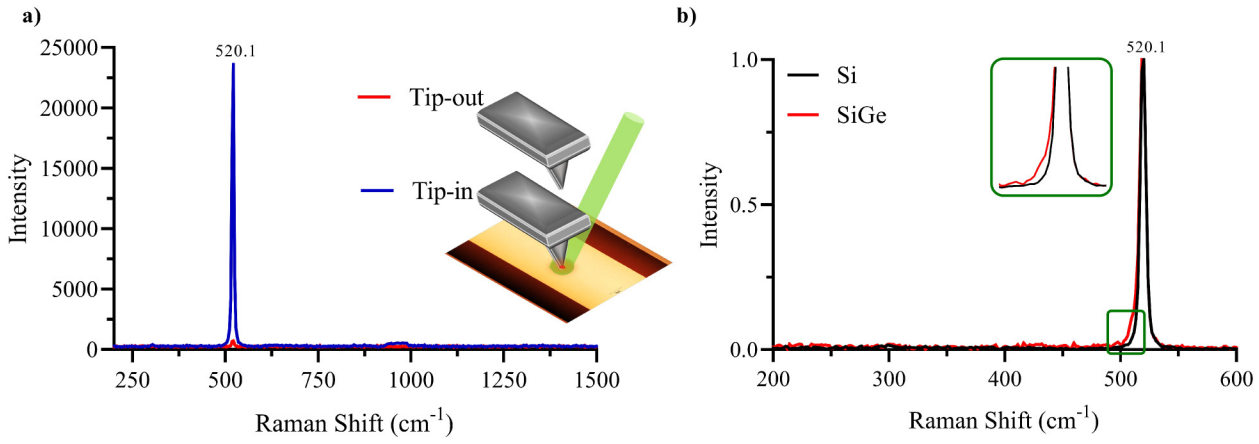

Figure 3. (a) Comparison between tip-in (blue) and tip-out (red) TERS spectra on SiGe region (in the insert, a schematic representation of tip-in/tip-out configuration); (b) comparison between tip-in point acquisitions collected with 532 nm laser on the relaxed (black) and strained-silicon (red) regions, shown in detail in the insert.

denoted as A_{far} and A_{near}, respectively. The radius of the excitation laser beam spot (r_{laser}) depends on several factors, which include the NA of the objective used and the TERS configuration employed. Considering the side-illumination of the current setup and the 50× long-working distance objective, the laser spot can be assumed to be $r_{laser} \approx 2$ μm. The tip radius is defined by the producer, and it is unrelated to the coating thickness. For the innovative probe employed, the radius is nominally identified to be $r_{tip} \approx 10$ nm. With these values, the EF can be evaluated through Eq. 4:

$$EF_{(SiGe)} = C\left(\frac{A_{far}}{A_{near}}\right) = C \times \frac{\pi \cdot r_{laser}^2}{\pi \cdot r_{tip}^2} \approx 1.769 \times 10^6 \quad (4)$$

The result shows that with the values taken into consideration, the TERS setup achieves a signal amplification of six orders of magnitude thanks to the combination of localized surface plasmonic resonance and the lightning rod effect, which led to an enhancement of the electromagnetic field in the closed region between the sample and the engaged tip.

However, it should be highlighted that the EF not only is strongly influenced by the wavelength of the excitation light used, but its calculation involves several non-negligible approximations that take into account unavoidable errors due to both r_{laser} and r_{tip}. The excitation laser spot geometry and radius can just be approximated as already described, considering that the TERS setup employed is in-side illumination. In addition, even though the probes' datasheet from the producer company is undebatable, the plasmonic tip radius during the acquisition is far from being precisely known: several processes mandatory to the measurement (such as the laser-tip alignment or the test acquisitions) can largely affect the shape and the diameter of the tip's apex. For the reasons explained, we consider contrast to be a more reliable parameter than EF, which turns out to have a higher value than expected.[21,49–51]

Once confirmed, the TERS performances on a point, localized acquisition, a map has been acquired around the edge between the SiGe and Si regions (Figure 4a) in order to test the lateral resolution of the setup. The acquisition consists of 192 points with a step size of 195 nm, acquired with the same parameters already described. Lorentzian fittings have been performed on the map in order to extract the information needed, i.e., strained and unstrained silicon peak positions and width. The first step of the fitting process involved the use of a single Lorentzian curve (Figure S3, Supplemental Material), given the overall symmetry of the main silicon peak at ≈520 cm^{-1}.

In Figure 4b, the hyperspectral map of the distribution of the full width half-maximum (FWHM) of all the acquired spectra is shown: the main silicon band results wider in the SiGe region, while it becomes sharper in the relaxed silicon case. The FWHM trend reflects very accurately the structure of the sample, but the single curve fitting does not represent the overall map, mostly in the SiGe portion of the acquisition, where a weak signal appears below the one at ≈520 cm^{-1}. This observation explains why the FWHM results are higher in the strained region. In order to account for the differences between Si and SiGe regions in terms of the spectra line shape, the acquisitions have been averaged with respect to the columns of the map, i.e., it is performed in a region where the homogeneity of the signal along the direction parallel to the fins is guaranteed, so the average procedure does not nullify the signal content. Forty-eight spectra result from this procedure, each one being the average of four spectra. With a careful look at these spectra, the required fitting procedure changes dramatically between relaxed (Si) and strained (SiGe) regions: in the first case, two Lorentzian curves are needed for an accurate reproduction of the spectra (for two peaks at ≈520.5 and ≈518.4 cm^{-1}, both coming from the unstrained-Si region), while in the second case there is an additional signal to take into account (in total three peaks: two at ≈520.5 and ≈517.8 cm^{-1} for the relaxed-Si, and one at ≈515.6 cm^{-1}, referred as the strained-Si peak).[52,53] As already said previously in the μ-Raman characterization section, the peak at ≈518.4 cm^{-1}, detected also in the unstrained-Si region spectra, is presumably due to the various manufacturing and epitaxial growth processes, that can induce an impure and imperfect crystal silicon structure. The TERS fitting procedures are reported in the spectra shown in Figure S4 (Supplemental Material).

In Figure 4c, the values of the sum of the areas related to the peaks at ≈520.5 and ≈518 cm^{-1} of each averaged spectrum are reported with respect to the positions of the acquired points: this parameter reproduces accurately the shape of the SiGe and Si regions along the map. In particular, the averaged acquisitions from point 25 on (green point), i.e., the first point acquired in the pure silicon region, show how the area tends to grow rapidly, demonstrating how the content of those spectra derives only from the two peaks considered and there is no longer any influence from the strained-Si peak. The presence of the strain-shifted Si peak in the SiGe region is steady, as can be seen from the trends in the plots in Figures 4d and 4e. More in particular, in the first figure, the value of the Raman shift of the band of the strained-Si peak has been plotted with respect to the acquisition position of the points along *x*. All the values acquired in the SiGe region up to point 24 (i.e., the last one inside the strained region) oscillate between the values 515.2 and 516.1 cm^{-1} of the Raman shift. From point 25 onwards, once the boundary is passed, its value tends to zero, since the strained-Si peak is no longer detected. The strained-Si peak does not disappear right after the boundary is crossed: in the pure silicon region, there is a residual strain induced by the fabrication process, since the epitaxial growth can produce minimal diffusion of strain at the edge.

The same interpretation can be applied to the plot in Figure 4e, where the trend of the value of the area of the strained Si peak has been plotted with respect to the acquisition position along *x*. As expected, the result is similar to

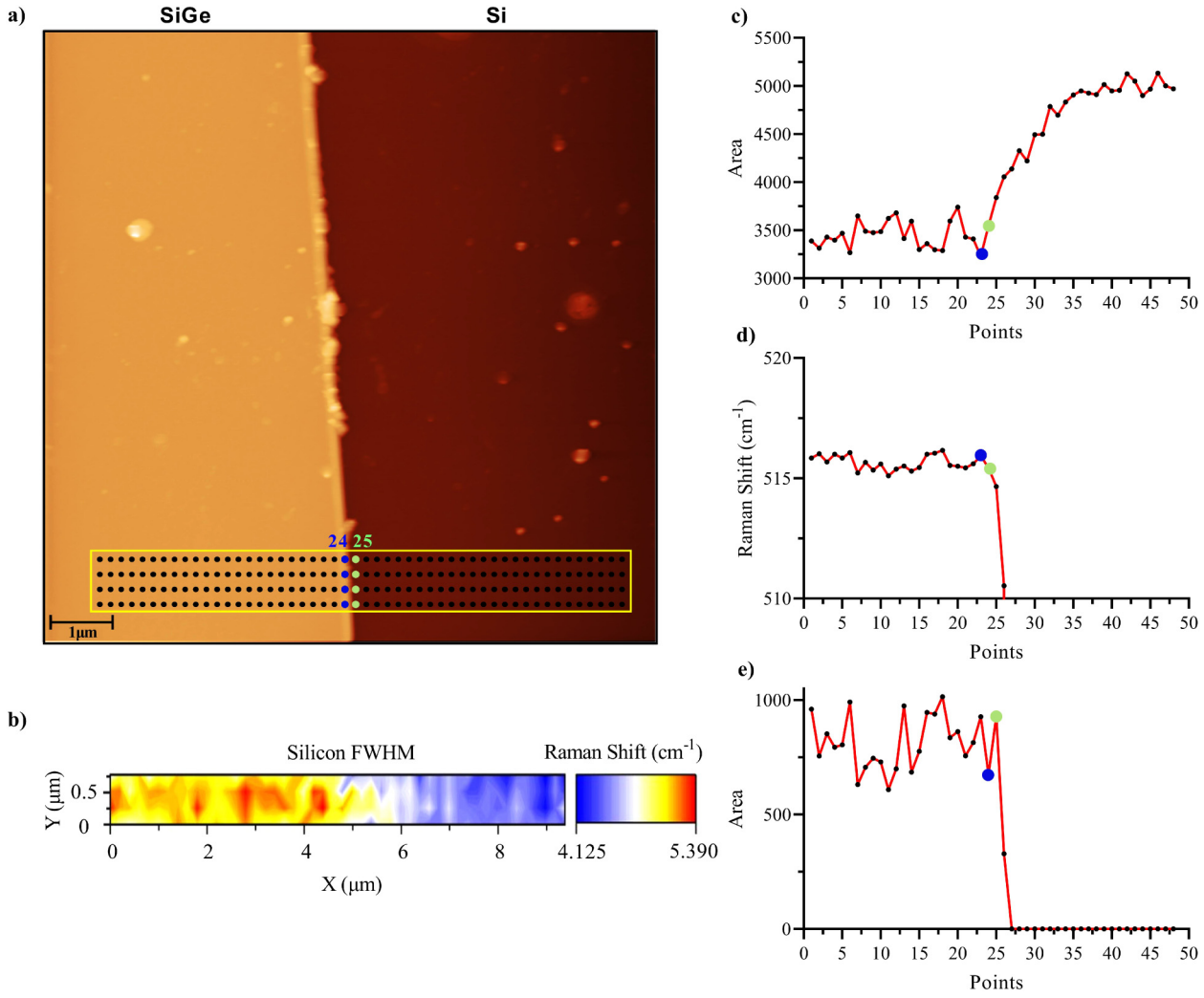

Figure 4. (a) Tip-enhanced Raman spectroscopy (TERS) map on a 10 × 10 µm^2 AFM topography acquired on the edge between the SiGe and Si regions of the SiGe epitaxial-on-SOI device based on 192 points with a distance between each point of 195 nm (the blue and green points represent the positions 24 and 25, respectively); (b) FWHM hyperspectral map obtained by performing a single Lorentzian curve fitting on all the acquisitions; (c) plot of the values of the sum of the areas (peaks at ≈520.5 and ≈ 518 cm^{-1}) obtained by performing a two and three Lorentzian curves fitting to the averaged spectra for the Si and SiGe region, respectively; (d) plot of the spectral position of the strained-Si peak of each averaged spectra; (e) plot of the value of the area of strained-Si peaks of each averaged spectra.

that obtained in Figure 4d in which once the edge is crossed, the area quickly saturates to zero, since the strained-Si peak is not detectable anymore.

Conclusion

The paper outlines the potential and reliability of the TERS technique for the characterization of modern semiconductor devices in the context of strained silicon technology, more in particular a SiGe epitaxial-on-SOI device as a case study. µ-Raman provides valuable insights about the strain of a SiGe layer grown on SiO_2 substrates, regardless of its thicknesses and germanium content, but at the same time the achievable lateral resolution is constrained by diffraction limits; on the other hand, the results obtained showed how TERS not only allows one to collect higher signal from the sample (when comparing tip-in and tip-out acquisitions), but also exhibits the sensitivity to the sample surface. In addition to that, TERS proved to be a powerful non-contact and non-destructive technique capable of overcoming the diffraction limit, offering high lateral resolution, and providing detailed insights into strain-induced deformations of crystal lattices. As a matter of fact, TERS in this case study demonstrated to be able to detect the signal related to the strain within the device a few nanometers deep in the SiGe layer, and to distinguish the relaxed region from the strained one with two-point acquisitions of just 195 nm apart. This result allows us to state that the lateral resolution obtained with TERS, in particular on samples of this type, unlocks the resolution capacity of the standard µ-Raman technique. In

addition to what has been said, TERS can also simultaneously provide chemical information linked to the topographical structure of the sample through AFM scans, thus allowing a rapid assessment of the outcome of the production process of the sample at the micro–nanometer scale. The results obtained demonstrate how TERS can potentially be an in-line integrated technique for direct and real-time monitoring of the outcome of semiconductor manufacturers, allowing reliable analysis and quality control of the products during the several steps of micro- and nano-electronic device production. Furthermore, we have confirmed that the TiN-coated TERS tips, designed for clean room environments, offer high performance in terms of signal amplification, making them an ideal solution for real-time quality control in micro- and nano-electronics manufacturing facilities.

Despite the demonstrated huge potential of strain induced in the silicon crystal structure, its integration into the complementary metal–oxide semiconductor manufacturing industry is hampered by the lack of real-time characterization tools. Currently, stress/strain values are predetermined during the product design; once the stress is externally induced, the strain percentage in the final product is then revealed indirectly through electrical measurements or functional testing. An in-line TERS-based system for real-time measurements can have a decisive impact on the early detection of structural defects induced in a device during the production process, reducing its costs and optimizing its yield and performances, but mostly avoiding the need to resort to external characterization tools outside the clean room or to destructive analyses.

Acknowledgments

Special acknowledgment is due to ScanSens GmbH, a partner within the European CHALLENGES project, who played an important role by providing TERS tips, without which the experimental phase of this research would not have produced these results.

Declaration of Conflicting Interests

The authors declared no potential conflicts of interest with respect to the research, authorship, and/or publication of this article.

Funding

The authors disclose the support for the research, authorship, and publication of this article as follows. This research was mainly carried out with the financial support of the project CHALLENGES (real-time nano CHAracterization reLatEd techNoloGiES), granted by the EU Horizon 2020 Research and Innovation Programme (Call H2020-NMBP-TO-IND-2019, Grant agreement no. 861857). The views and opinions expressed are those of the authors and do not necessarily reflect those of the European Union. Neither the European Union nor the granting authority can be held responsible for them. In addition, the research was partially carried out at the Platform for Nanocharacterisation (PFNC) and supported by the programs "Recherche Technologique de Base" and "France 2030 - ANR-22-PEEL-0014" of the French National Research Agency (ANR).

ORCID iDs

Giancarlo La Penna https://orcid.org/0000-0003-1065-7164
Narciso Gambacorti https://orcid.org/0009-0009-6543-1163
Jérôme Richy https://orcid.org/0000-0002-6543-3670

Supplemental Material

All supplemental material mentioned in the text is available in the online version of the journal.

References

1. R. Quhe, L. Xu, S. Liu, C. Yang, et al. "Sub-10 nm Two-Dimensional Transistors: Theory and Experiment". Phys. Rep. 2021. 938: 1–72. 10.1016/j.physrep.2021.07.006
2. S.W. Bedell, A. Khakifirooz, D.K. Sadana. "Strain Scaling for CMOS". MRS Bull. 2014. 39: 131–137. 10.1557/mrs.2014.5
3. H.H. Radamson, X. He, Q. Zhang, J. Liu, et al. "Miniaturization of CMOS". Micromachines. 2019. 10(5): 293. 10.3390/mi10050293
4. S.E. Thompson, G. Sun, Y.S. Choi, T. Nishida. "Uniaxial-Process-Induced Strained-Si: Extending the CMOS Roadmap". IEEE Trans. Electron Devices. 2006. 53(5): 1010–1020. 10.1109/TED.2006.872088
5. M.V. Fischetti, S.E. Laux. "Band Structure, Deformation Potentials, and Carrier Mobility in Strained Si, Ge, and SiGe Alloys". J. Appl. Phys. 1996. 80(4): 2234–2252. 10.1063/1.363052
6. A. Bonnevialle, S. Reboh, C. Le Royer, Y. Morand, et al. "On the Use of a Localized STRASS Technique to Obtain Highly Tensile Strained Si Regions in Advanced FDSOI CMOS Devices". Phys. Status Solidi C. 2016. 13(10–12): 740–745. 10.1002/pssc.201600028
7. P.F. Morin, L. Grenouillet, N. Loubet, A. Pofelski, et al. "Mechanical Analyses of Extended and Localized UTBB Stressors Formed with Ge Enrichment Techniques". ECS Trans. 2015. 66(4): 57. 10.1149/06604.0057ecst
8. D. Cooper, T. Denneulin, N. Bernier, A. Béché, J.-L. Rouvière. "Strain Mapping of Semiconductor Specimens with nm-Scale Resolution in a Transmission Electron Microscope". Micron. 2016. 80: 145–165. 10.1016/J.Micron.2015.09.001
9. D. Cooper, T. Denneulin, J.-P. Barnes, J.-M. Hartmann, et al. "Strain Mapping with nm-Scale Resolution for the Silicon-on-Insulator Generation of Semiconductor Devices by Advanced Electron Microscopy". J. Appl. Phys. 2012. 112: 124505. 10.1063/1.4767925
10. V.V. Hoang, Y.J. Cho, J.H. Yoo, J.-M. Yang, et al. "2D Strain Measurement in Sub-10 nm SiGe Layer with Dark-Field Electron Holography". Curr. Appl. Phys. 2015. 15(11): 1529–1533. 10.1016/j.cap.2015.09.001
11. A. Durand, M. Kaufling, D. Le-Cunff, D. Rouchon, P. Gergaud. "In-Line Monitoring of Strain Distribution Using High Resolution X-ray Reciprocal Space Mapping into 20 nm SiGe pMOS". Mater. Sci. Semicond. Process. 2017. 70: 99–104. 10.1016/J.Mssp.2016.12.003
12. A. Schulze, R. Loo, L. Witters, H. Mertens, et al. "Strain and Compositional Analysis of (Si)Ge Fin Structures Using High Resolution X-ray Diffraction". Phys. Status Solidi C. 2017. 14 (12): 1700156. 10.1002/Pssc.201700156
13. J.R. Holt, A. Madan, E.C.T. Harley, M.W. Stoker, et al. "Observation of Semiconductor Device Channel Strain Using

In-Line High Resolution X-ray Diffraction". J. Appl. Phys. 2013. 114: 154502. 10.1063/1.4824819
14. S.H. Olsen, P. Dobrosz, R.M.B. Agaiby, Y.L. Tsang, et al. "Nanoscale Strain Characterisation for Ultimate CMOS and Beyond". Mater. Sci. Semicond. Process. 2008. 11(5–6): 271–278. 10.1016/J.Mssp.2009.06.003
15. M.A. Lauterbach. "Finding, Defining and Breaking the Diffraction Barrier in Microscopy: A Historical Perspective". Opt. Nanoscopy. 2012. 1: 8. 10.1186/2192-2853-1-8
16. J. Wessel. "Surface-Enhanced Optical Microscopy". J. Opt. Soc. Am. B. 1985. 2(9): 1538–1541. 10.1364/JOSAB.2.001538
17. R.M. Stockle, Y.D. Suh, V. Deckert, R. Zenobi. "Nanoscale Chemical Analysis by Tip-Enhanced Raman Spectroscopy". Chem. Phys. Lett. 2000. 318: 131–136. 10.1016/S0009-2614(99)01451-7
18. N. Hayazawa, Y. Inouye, Z. Sekkat, S. Kawata. "Metallized Tip Amplification of Near-Field Raman Scattering". Opt. Commun. 2000. 183: 333–336. 10.1016/S0030-4018(00)00894-4
19. M.S. Anderson. "Locally Enhanced Raman Spectroscopy with an Atomic Force Microscope". Appl. Phys. Lett. 2000. 76: 3130–3132. 10.1063/1.126546
20. B. Pettinger, G. Picardi, R. Schuster, G. Ertl. "Surface Enhanced Raman Spectroscopy: Towards Single Molecular Spectroscopy". Electrochemistry. 2000. 68: 942–949. 10.5796/electrochemistry.68.942
21. K.F. Gibson, S.G. Kazarian, S.S. Kharintsev. "Tip-Enhanced Raman Spectroscopy". In: R.A. Meyers, editor. Encyclopedia of Analytical Chemistry: Applications, Theory, and Instrumentation. Chichester, UK: Wiley, 2020. Pp. 1-33. doi:10.1002/9780470027318.A9278.Pub2.
22. N. Kumar, S. Mignuzzi, W. Su, D. Roy. "Tip-Enhanced Raman Spectroscopy: Principles and Applications". EPJ Techn. Instrum. 2015. 2: 9. 10.1140/epjti/s40485-015-0019-5
23. W. Su, N. Kumar, S. Mignuzzi, J. Crain, D. Roy. "Nanoscale Mapping of Excitonic Processes in Single-Layer MoS_2 Using Tip-Enhanced Photoluminescence Microscopy". Nanoscale. 2016. 8: 10564–10569. 10.1039/C5NR07378B
24. W. Su, N. Kumar, H. Shu, O. Lancry, M. Chaigneau. "In Situ Visualization of Optoelectronic Behavior of Grain Boundaries in Monolayer WSe_2 at the Nanoscale". J. Phys. Chem. C. 2021. 125(48): 26883–26891. 10.1021/acs.jpcc.1c08064
25. N. Kumar, A. Zoladek-Lemanczyk, A.A.Y. Guilbert, W. Su, et al. "Simultaneous Topographical, Electrical and Optical Microscopy of Optoelectronic Devices at the Nanoscale". Nanoscale. 2017. 9(8): 2723–2731. 10.1039/C6NR09057E
26. P. Verma. "Tip-Enhanced Raman Spectroscopy: Technique and Recent Advances". Chem. Rev. 2017. 117(9): 6447–6466. 10.1021/acs.chemrev.6b00821
27. Z. Zhang, S. Sheng, R. Wang, M. Sun. "Tip-Enhanced Raman Spectroscopy". Anal. Chem. 2016. 88(19): 9328–9346. 10.1021/acs.analchem.6b02093
28. S.S. Kharintsev, A.V. Kharitonov, S.K. Saikin, A.M. Alekseev, S. G. Kazarian. "Nonlinear Raman Effects Enhanced by Surface Plasmon Excitation in Planar Refractory Nanoantennas". Nano Lett. 2017. 17(9): 5533–5539. 10.1021/acs.nanolett.7b02252
29. Cortie M.B., J. Giddings, A. Dowd. "Optical Properties and Plasmon Resonances of Titanium Nitride Nanostructures". Nanotechnology. 2010. 21(11): 115201. 10.1088/0957-4484/21/11/115201
30. G.V. Naik, J.L. Schroeder, X. Ni, A.V. Kildishev, et al. "Titanium Nitride as a Plasmonic Material for Visible and Near-Infrared Wavelengths". Opt. Mater. Express. 2012. 2(4): 478–489. 10.1364/OME.2.000478
31. J.D. Scherger, E.A. Evans, J.A. Dura, M.D. Foster. "Extending Nanoscale Spectroscopy with Titanium Nitride Probes". J. Raman Spectrosc. 2016. 47: 1332–1336. 10.1002/jrs.4959
32. J.D. Scherger, M.D. Foster. "Tunable, Liquid Resistant Tip Enhanced Raman Spectroscopy Probes: Toward Label-Free Nano-Resolved Imaging of Biological Systems". Langmuir. 2017. 33(31): 7818–7825. 10.1021/acs.langmuir.7b01338
33. A. Lucia, O. Antonino Cacioppo, E. Iulianella, L. Latessa, et al. "Capability of Tip-Enhanced Raman Spectroscopy About Nanoscale Analysis of Strained Silicon for Semiconductor Devices Production". Appl. Phys. Lett. 2017. 110(10): 103105. 10.1063/1.4978261
34. T.S. Perova, R.A. Moore, K. Lyutovich, M. Oehme, E. Kasper. "Strain, Composition and Crystalline Perfection in Thin SiGe Layers Studied by Raman Spectroscopy". Thin Solid Films. 2008. 517(1): 265–268. 10.1016/j.tsf.2008.08.060
35. D. Rouchon, M. Mermoux, F. Bertin, J.M. Hartmann. "Germanium Content and Strain in $Si_{1-x}Ge_x$ Alloys Characterized by Raman Spectroscopy". J. Cryst. Growth. 2014. 392: 66–73. 10.1016/j.jcrysgro.2014.01.019
36. A. Durand, D. Rouchon, D. Le-Cunff, P. Gergaud. "Micro-Raman Spectroscopy as a Complementary Technique to High Resolution X-ray Diffraction for the Characterization of $Si_{1-x}Ge_x$ Thin Layers". Phys. Status Solidi C. 2015. 12(3): 304–309. 10.1002/pssc.201400113
37. W.J. Brya, "Raman Scattering in Ge–Si Alloys". Solid State Commun. 1973. 12(4): 253–257. 10.1016/0038-1098(73)90692-3
38. J.C. Tsang, P.M. Mooney, F. Dacol, J.O. Chu. "Measurements of Alloy Composition and Strain in Thin Ge_xSi_{1-x} Layers". J. Appl. Phys. 1994. 75(12): 8098–8108. 10.1063/1.356554
39. H.K. Shin, D.J. Lockwood, J.M. Baribeau. "Strain in Coherent-Wave SiGe/Si Superlattices". Solid State Commun. 2000. 114(10): 505–510. 10.1016/S0038-1098(00)00111-3
40. M.I. Alonso, K. Winer. "Raman Spectra of C-$Si_{1-x}Ge_x$ Alloys". Phys. Rev. B. 1989. 39(14): 10056–10062. 10.1103/physrevb.39.10056
41. F. Pezzoli, E. Bonera, E. Grilli, M. Guzzi, et al. "Raman Spectroscopy Determination of Composition and Strain in $Si_{1-x}Ge_x$/Si Heterostructures". Mater. Sci. Semicond. Process. 2008. 11(5–6): 279–284. 10.1016/j.mssp.2008.09.012
42. M. Cazayous, J. Groenen, F. Demangeot, R. Sirvin, et al. "Strain and Composition in Self-Assembled SiGe Islands by Raman Spectroscopy". J. Appl. Phys. 2002. 91: 6772–6774. 10.1063/1.1469200
43. Y.F. Tzeng, S. Ku, S. Chang, C.M. Yang, et al. "Noncontact, In-Line Measurement of Boron Concentration from Ultrathin Boron-Doped Epitaxial $Si_{1-x}Ge_x$ Layers on Si (100) by Multiwavelength Micro-Raman Spectroscopy". J. Mater. Res. 2011. 26: 739–744. 10.1557/jmr.2010.62
44. T.S. Perova, J. Wasyluk, K. Lyutovich, E. Kasper, et al. "Composition and Strain in Thin $Si_{1-x}Ge_x$ Virtual Substrates Measured by Micro-Raman Spectroscopy and X-ray Diffraction". J. Appl. Phys. 2011. 109(3): 033502. 10.1063/1.3536508

45. P. Dobrosz, S.J. Bull, S.H. Olsen, A.G. O'Neill. "The Use of Raman Spectroscopy to Identify Strain and Strain Relaxation in Strained Si/SiGe Structures". Surf. Coat. Technol. 2005. 200 (5–6): 1755–1760. 10.1016/J.Surfcoat.2005.08.048
46. M. Roelke, M. Hecker, P. Hermann, D. Lehninger, et al. "Surface-Sensitive Strain Analysis of Si/SiGe Line Structures by Raman and UV–Raman Spectroscopy". Proc. SPIE 7405, Instrumentation, Metrology, and Standards for Nanomanufacturing III. 2009. 7405: 74050S. 10.1117/12.830866
47. M. Kadlečíková, Ľ. Vančo, J. Breza, M. Mikolášek, et al. "Raman Spectroscopy of Silicon with Nanostructured Surface". Optik. 2022. 257: 168869. 10.1016/j.ijleo.2022.168869
48. A. Picco, E. Bonera, E. Grilli, M. Guzzi, et al. "Raman Efficiency in SiGe Alloys". Phys. Rev. B. 2010. 82: 115317. 10.1103/physrevb.82.115317
49. N. Kumar, A. Rae, D. Roy. "Accurate Measurement of Enhancement Factor in Tip-Enhanced Raman Spectroscopy Through Elimination of Far-Field Artefacts". Appl. Phys. Lett. 2014. 104(12): 123106. 10.1063/1.4869184
50. A. Tarun, N. Hayazawa, S. Kawata. "Tip-Enhanced Raman Spectroscopy for Nanoscale Strain Characterization". Anal. Bioanal. Chem. 2009. 394: 1775–1785. 10.1007/S00216-009-2771-3
51. J. Stadler, T. Schmid, R. Zenobi. "Developments in and Practical Guidelines for Tip-Enhanced Raman Spectroscopy". Nanoscale. 2012. 4:1856–1870. 10.1039/C1NR11143D
52. P. Hermann, M. Hecker, D. Chumakov, M. Weisheit, et al. "Imaging and Strain Analysis of Nano-Scale SiGe Structures by Tip-Enhanced Raman Spectroscopy". Ultramicroscopy. 2011. 111(11): 1630–1635. 10.1016/j.ultramic.2011.08.009
53. N. Hayazawa, M. Motohashi, Y. Saito, S. Kawata. "Characterization of Localized Strain of Crystals in Nano-Scale by Tip-Enhanced Raman Spectroscope and Microscope". Proc. SPIE 2007. 6769: 67690P. 10.1117/12.733468